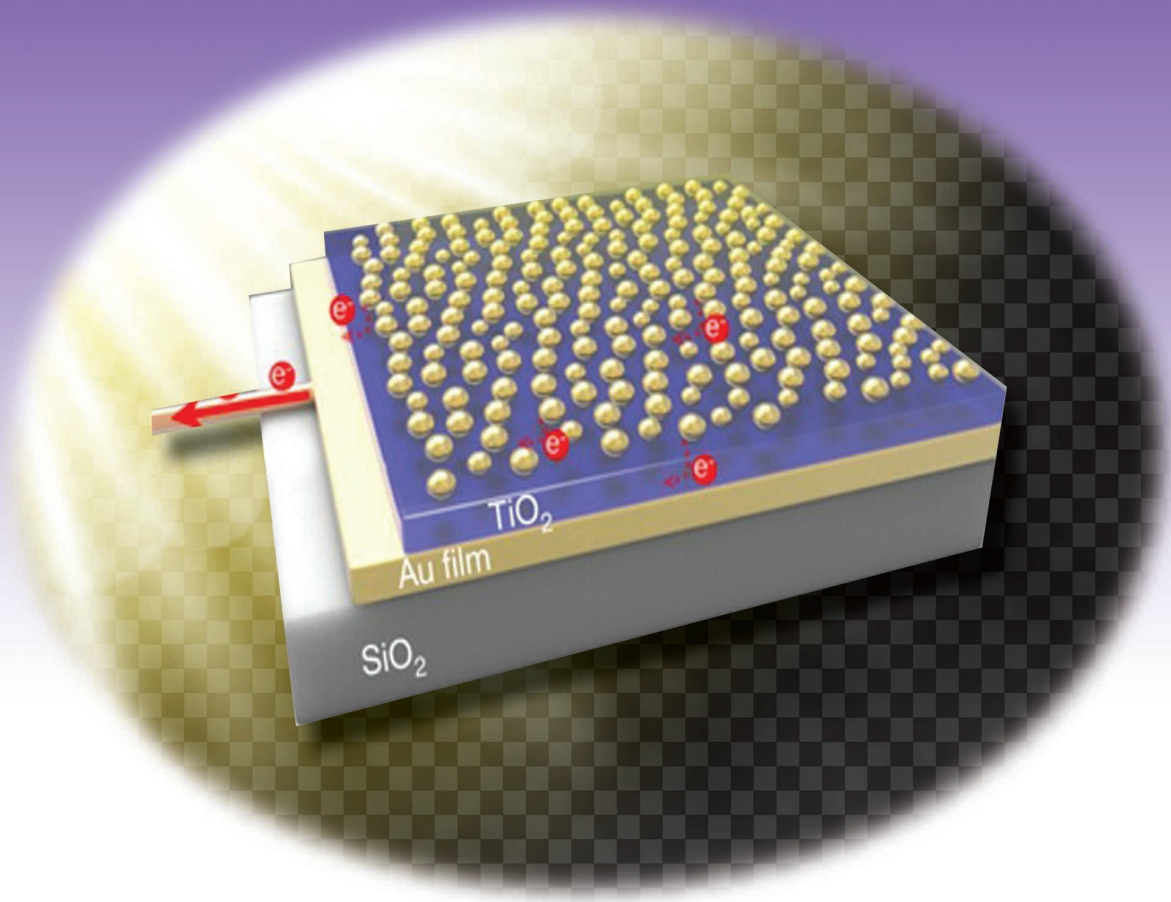

BACKGROUND—©ISTOCKPHOTO.COM/EGOR SUVOROV

Strong Interference in Planar, Multilayer Perfect Absorbers

Achieving high-operational performances in visible and near-infrared regimes.

AMIR GHOBADI, HODJAT HAJIAN, BAYRAM BUTUN, AND EKMEL OZBAY

LIGHT-MATTER INTERACTIONS at subwavelength-designed nanostructures have been the subject of intensive study in recent years. The realization of an ideal "blackbody" absorber is an emerging topic in nanophotonics and nanoplasmonics. An ideal black absorber is an object that harvests incoming light with near-unity efficiency. Based on their absorption spectral coverage, they are classified as narrow-band or broadband absorbers. This requirement can be achieved in bulky designs that have a thickness much larger than its light penetration depth as well as antireflective surface texturing.

For optoelectronic applications, however, it is essential to acquire this strong absorption in dimensions much

Digital Object Identifier 10.1109/MNANO.2019.2916113
Date of publication: 10 June 2019

1932-4510/19©2019IEEE

smaller than the light wavelength, which are comparable to the carrier's diffusion length. In this manner, the collection probability of photo-generated carriers will be enhanced. Therefore, the main goal in nanophotonics-based absorbers is to design an optically thick, but electrically thin, device. The most frequently employed solution for this contradiction is through the use of nanostructures with specific absorption properties. Properly designed metal and semiconductor nanostructures can confine the incoming light in subwavelength geometries and fully harvest it. These periodic nanounits couple light into the ultrathin active layer. Although these design configurations have promising optical properties, their upscaling is mainly restricted by their complex fabrication route.

Subwavelength nanoresonant units generally require electron beam lithography (EBL), which is not a large-scale, compatible-synthesis approach. As a result, in recent years, researchers have focused on developing planar, multilayer designs for light-perfect absorption. Strong interference effects in these ultrathin multilayers provide an efficient light-matter interaction in lithography-free architectures. These lithography-free planar absorbers are achieved in a variety of material types, including metals and semiconductors.

Subwavelength nanoresonant units generally require electron beam lithography, which is not a large-scale, compatible-synthesis approach.

LITHOGRAPHY-FREE, MULTILAYER PERFECT ABSORBERS

Near-unity absorption is achieved in all parts of the electromagnetic (EM) spectrum [1] when proper materials and design configurations are used. The materials utilized most frequently are metals, which are classified into two main categories: noble metals, e.g., gold (Au), silver (Ag), and platinum (Pt), and lossy metals such as titanium (Ti), chromium (Cr), and tungsten (W). Inherently, surface plasmon resonance (SPR) in plasmonic noble metals has narrow spectral coverage. To extend the absorption bandwidth (BW), various strategies such as the use of multidimensional/multishaped units and elongated shapes [2]–[10], replacement with a lossy component, and elongated, double-resonant units have been proposed [11]–[16]. However, as stated previously, all of these designs have nanostructured, ultrasmall shapes that are fabricated by using the EBL process.

In recent work, we theoretically demonstrated that noble metals can offer strong absorption in ultraviolet and visible (Vis) parts of the EM spectrum, while lossy metals can extend the upper-absorption edge up to the near-infrared (NIR) region [1]. Experimentally, these findings have been demonstrated in many recent research studies [17]–[44]. In one pioneering study, Mattiucci et al. showed that impedance matched with thin metamaterials make metals absorbent [26]. They proved that the periodic arrangement of metal–insulator (MI) pairs provides light-perfect absorption in an ultrabroadband wavelength regime and indicated that increasing the number of MI pairs could extend the absorption BW.

As a common example of MI pair-based designs, Li et al. proposed a Cr-silicon dioxide (SiO_2)-Cr MI–metal (MIM)-based absorber that provides a greater than 0.9 absorption rate in the 450–850-nm wavelength range [24]; this BW is a limitation for most metals [1]. According to our theoretical findings, ideal absorption characteristics can be broadened if the effective permittivity of the metal layer is reduced. A solution for this is to make a composition that has a low-permittivity medium, such as air. To keep the overall process EBL-free, we adopted an approach based on dewetting to tune the filling fraction of nanoholes [45]. As a result of this modification, near-unity absorption was achieved from 400 to 1,150 nm. To further enhance the absorption BW, the MIM cavity design can be replaced by a symmetric MIM–insulator (MIMI) design. In this type of design configuration, the top insulation layer acts as a broadband antireflective coating that couples the incident light into the underneath MIM cavity.

Recently, different combinations of metal and insulator layers were used to substantiate the absorption BW. Deng et al. showed that the highest absorption response can be achieved in an $Au\text{-}SiO_2\text{-}Cr\text{-}SiO_2$ design where the absorption says above 0.9 in an ultrabroadband range of 400–1,400 nm [28]. To further boost the absorption BW of these MIMI designs, different strategies were employed, e.g., surface texturing [35], disordered plasmonic nanohole patterns [36], and optimization of the reflector material [37]. However, these modifications do not adequately improve the absorption upper edge. Even using a larger number of $[MI]_N$ pairs (e.g., 16 pairs) cannot significantly substantiate the BW [32]. In a recent article, our group revealed an extraordinary optical response of bismuth (Bi) metal in light-perfect absorption [46]. We experimentally demonstrated a near-unity average absorption from 500 to 2,500 nm, which is the largest reported BW for a planar MI pair-based design to date. Other chemical-based synthesis methods have also been employed to obtain ultrabroadband perfect absorbers, but our main focus for this article is the planar-trapping schemes.

Similar to metals, this strong, interference-based light harvesting can also be acquired in ultrathin, semiconductor layers, the main difference of which is its operation spectral coverage. Metals have an extinction coefficient in the whole EM spectrum, while semiconductors can only absorb photons with energies above their optical band gap. In fact, perfect semiconductor, multilayer-based absorbers have a longer history. In 2012, researchers from Capasso's group demonstrated a strong absorption property

in an Au-germanium (Ge)-based metal–semiconductor (MS) design [47]. By changing the Ge-layer thickness, the absorption peak position can be tuned. This strong, light-matter interaction can lead to exceeding the Yablonovitch limit [48]. Later studies demonstrated many different MS configurations that achieve stronger and broader light absorption [49]–[51]. This is of great interest in photoelectronic applications, which confine light in dimensions much smaller than the carrier's diffusion length.

In addition to MS designs, another promising configuration is based on metal–oxide–semiconductor (MOS) cavities. In these cavities, higher degrees of freedom are provided because of the spacer layers. Based on theoretical calculations [1], this configuration provides impedance matching in thinner semiconductor layers compared to that of MS designs. Several studies demonstrated strong absorption in ultrathin, semiconductor-based, MOS configurations [52], [53]. Another advantage of MOS design over MS structure is the electrical property of the oxide layer, which acts as an electron- or hole-transport layer to provide electron-hole pair separation at the semiconductor–oxide interface. This is an important factor in energy conversion applications, where the spatial separation of photogenerated carriers prolongs their lifetime. Moreover, the MOS cavity can be designed to provide spectrally selective light absorption.

Although MS and MOS design architectures lead to light harvesting in ultrathin, nanometer-scale semiconductor layers, they cannot support strong light-matter interactions in atomic-scale dimensions such as 2D semiconductors [1]. The recent emergence of 2D transition metal dichalcogenides (TMDs) such as molybdenum disulfide (MoS_2), offers promise for future atomic-scale optoelectronics. However, their ultrathin thickness causes poor optical performance in these types of TMDs. It is, therefore, essential to couple these 2D planes with light-trapping schemes that obtain broad and strong light absorption. As stated previously, strong, near-field coupling using plasmonic nanounits is one of these solutions [54], [55]; however, this article aims to summarize the planar multilayer trapping strategies. The proper architecture for light absorption in these 2D semiconductors is to couple them into 1D photonic crystals (PCs). PC-induced, strong-light intensities can significantly enhance light absorption in the monolayer of MoS_2 in both narrow and broad frequency ranges [56], [57].

The most common cavity designs for metal and semiconductor materials are summarized in Figure 1. Aside from metals and semiconductors, other types of materials such as alternative plasmonics and polar materials may also be used to obtain light-perfect absorption in the midinfrared and far-infrared regimes [58]–[64]; however, this article mainly focuses on Vis- and NIR-based perfect absorbers and addresses their potential applications.

PHOTOVOLTAICS AND PHOTODETECTION

Two of the most promising applications of light-perfect absorbers are photovoltaics (PVs) and photodetection. In PV solar cells, the incoming photon generates electron-hole pairs. After these pairs separate, they are transferred toward the contacts and create electricity in the output. As discussed previously, strong interference in MS and MOS cavities is an efficient approach for acquiring near-unity absorption in ultrathin semiconductor layers. In one significant study, Steenhoff et al. designed and fabricated an ultrathin, resonant-cavity-enhanced solar cell with a 13-nm-thick Ge active layer [65]. Their experimental characterizations showed a conversion efficiency as high as 3.6% in such a thin, absorbent layer. Considering the amorphous nature of the layer, which is made using simple, low-cost evaporation tools, this is a very promising design for upscaling. Generally, semiconductor layers with such thin thicknesses have an amorphous nature, and typically, an amorphous layer has a short diffusion length (i.e., 1–10 nm), which is why an efficient trapping scheme that harvests light in dimensions below the diffusion length is necessary. Clearly, a crystalline layer will be more efficient from an electrical perspective.

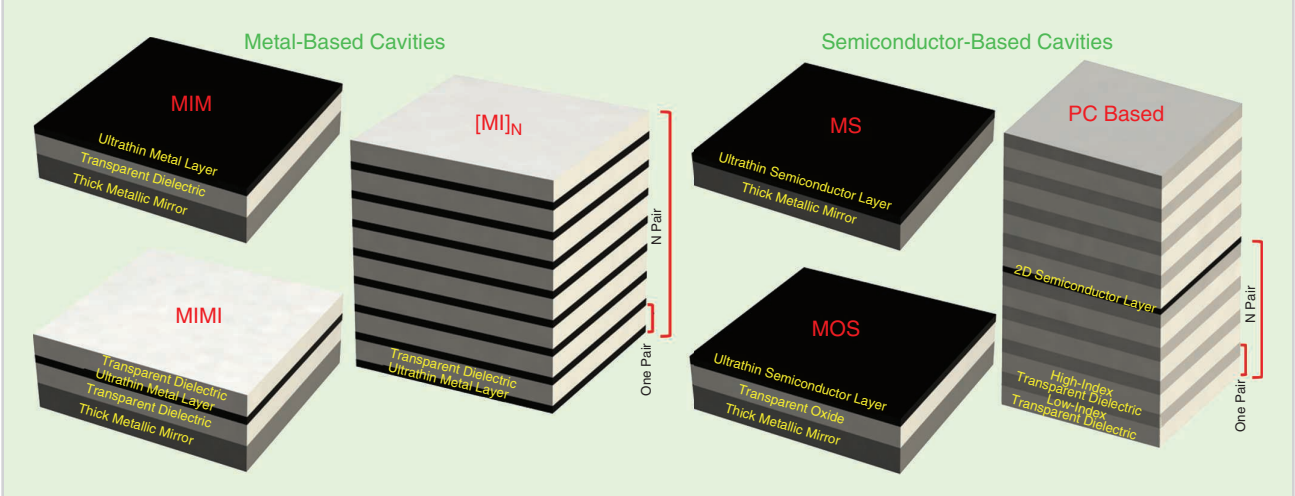

FIGURE 1 The most commonly used cavity designs for metal and semiconductor-based ultrathin absorbers.

One alternative for synthesizing crystalline layers in such thin dimensions is the chemical synthesis of organic semiconductors. Recently, an innovative design proposed by Liu and colleagues obtained a record efficiency of 11.1% in organic-based solar cells [66]. The proposed design and its current-voltage characteristics are shown in Figure 2. As mentioned previously, the overall performance of a photo-conversion device can be boosted upon enhancing the absorption BW and strength of the active layer. For this purpose, a series connection of cavities with double-resonance behavior was utilized. Moreover, a recent study presents a fabrication route that synthesizes nanometer-scale-thick, single-crystalline Ge coatings for spectrally selective photodetection [67]. Incorporating an ultrathin Ge layer on top of a predesigned MI cavity leads to the formation of a spectrally selective metal–insulator–semiconductor (MIS)-based photodetector, as depicted in Figure 3(a)–(c). By tuning the oxide- and semiconductor-layer thickness, the spectral position of the absorption peak can be tuned. Ultrathin thickness, strong absorption of the cavity, and the high crystalline quality of Ge leads to a highly efficient Vis light photodetector with high responsively, as shown in Figure 3(d).

A further enhancement of these designs' performance can be achieved by using ultrathin surface engineering, where the electrical response is improved significantly while the optical response stays intact [68]–[70]. Another innovative method to design a spectrally selective photodetector is using a planar cavity to transmit a portion of the EM spectrum. Butun et al. demonstrated amorphous, Si-based color photodetectors by monolithically integrating the Ag-SiO_2-Ag MIM cavity top contact [71]. By changing the middle spacer-layer thickness, the transmission profile of the MIM cavity can be tuned over the whole Vis spectrum.

Another area for the potential use of optical interference in PV cells is the design of semitransparent solar cells with vivid colors for outdoor decorative applications. As its name implies, the structure should be resonant in a specific wavelength and should pass the rest of the

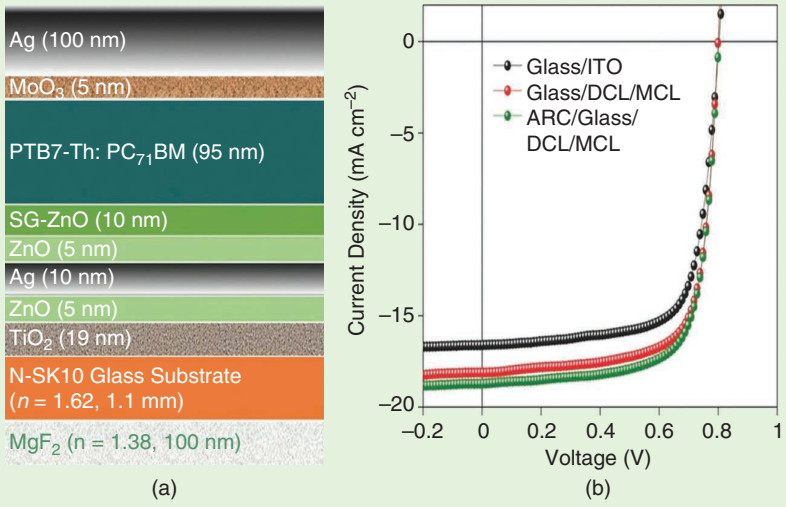

FIGURE 2 (a) A cascaded, cavity-based, organic solar cell and (b) its current-voltage characteristics under solar irradiation. (Used with permission from [66].) MoO_3: molybdenum trioxide; SG-ZnO: sol-gel zinc oxide; MGF_2: magnesium fluoride; PTB7-Th: PC_{71}BM:polymer blend; N-SK10: glass layer; ITO: indium-doped tin oxide; DCL: dielectric cavity layer; MCL: metallic cavity layer; ARC: antireflective coating.

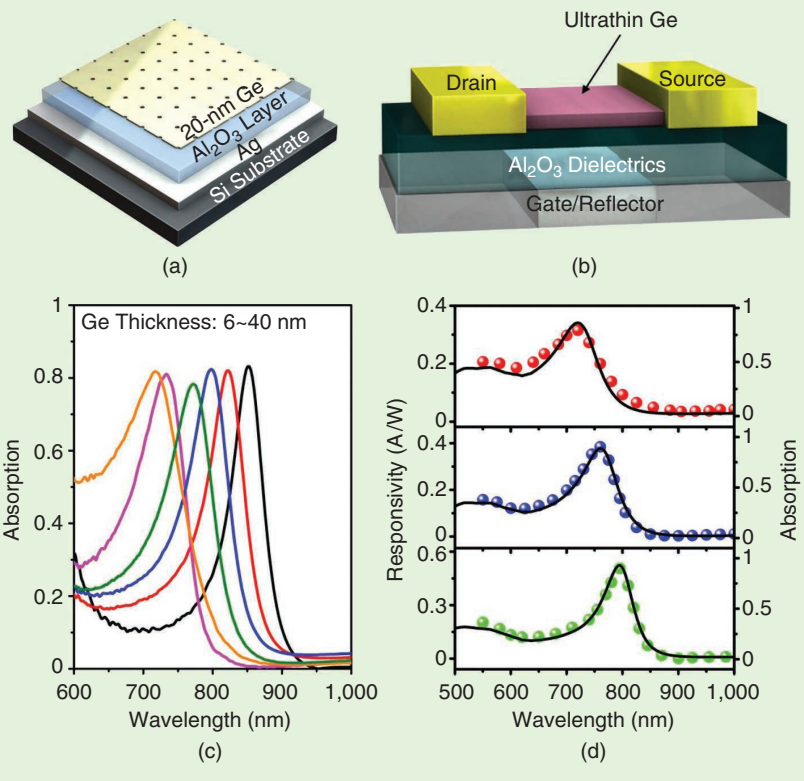

FIGURE 3 (a) The proposed Ge-based, MOS, cavity-perfect absorber design and (b) its utilization as a spectrally selective Vis light photodetector. (c) The absorption response of this cavity is a function of Ge layer thickness, while the bottom MI design geometry is fixed. (d) The responsivity of the fabricated MOS-based photodetector with three different Ge-layer thicknesses of 12, 17, and 26 nm, respectively. (Used with permission from [67].) Al_2O_3: aluminum oxide; A/W: ampere per watt.

spectrum. Therefore, the thickness of the active layer should be kept thin enough to provide light transmission. This resonant behavior can be easily acquired in an MS or MS metal (MSM)-cavity architecture.

According to earlier studies, an amorphous, Si-based color filter represents resonance in the Vis range in thicknesses below 25 nm [72]; however, in an amorphous, Si-based solar cell, the dopant layers alone already have a thickness of between 40 and 50 nm [73]. It is, therefore, very challenging to realize both characteristics at the same time, and for a colored, amorphous, Si-based solar cell, one should employ an ultrathin non-Si hole as well as electron transport layers. Lee et al. demonstrated a colorful, ultrathin PV cell made of a 10–27-nm-thick, amorphous, Si-based active layer embedded between a 10-nm indene-C_{60} bisadduct, and 8-nm V_2O_5 layers that act as electron- and hole-transport layers, respectively [74]. This multilayer structure is capped with an optically thick (120 nm) Ag bottom contact and a semitransparent 23-nm top contact. As such, the overall cavity acts as a narrow-band, reflective, Vis-light color filter where the thickness of an amorphous, Si-based layer tunes the spectral position of the reflection dip. To achieve yellow, magenta, and cyan colors, the amorphous, Si-based layer thicknesses of 10, 18, and 27 nm, respectively, were chosen. The bottom-layer thickness can be thinned down in a way that the overall solar cell becomes transparent. Doing so provides an opportunity to use these solar cells as a window in outdoor and indoor designs.

Because of their narrow spectral coverage, the overall power conversion efficiency in these solar cells was below 3%; however, the absorption BW of the design and the poor crystallinity of the amorphous, Si-based layer is responsible for this low solar cell efficiency. As mentioned previously, the solution for this deficiency is the synthesis of highly absorbing organic semiconductors. Liu et al. designed and fabricated a magenta-colored PV cell using 30-nm-thick perovskite (PVSK), i.e., $CH_3NH_3PbI_{3-x}Cl_x$, which shows remarkable efficiency as high as 11.5% [75]. The obtained efficiency for this colorful solar cell design is 75% of that of the black, thick cell (with a thickness of an order of magnitude larger), which highlights the potential of metasurface designs for colorful and efficient organic-based solar cells. The proposed design, its band alignment, and current-voltage characteristics are shown in Figure 4(a)–(c). There is a tradeoff between transparency level and solar cell efficiency, and as we increase the transmission amount, the efficiency drops [76].

A recent study on PVSK-based planar designs demonstrated an indium-doped tin oxide (ITO)-free design with a record efficiency of 14%. In this design, W trioxide (WO_3)/Ag/tin O_2(SnO_2) acts as a transparent contact with strong interference effects [77]. High-performance, see-through, PVSK solar cells producing angle-insensitive transmissive colors with high efficiency and high color purity, have been proved by employing optical microcavities incorporated with a phase-compensating, dielectric functional overlay [78]. Most of the light in this design is trapped within the solar cell cavity and in the specific color wavelength of red-green-blue (RGB), resulting in a relatively high transmittance. The color of the solar cell multilayer design is controlled using cavity thickness. The power conversion efficiency for the proposed RGB-colored solar cells were 10.47, 10.66, and 11.18%, respectively.

In addition, the bottom metal-based reflector can be changed using a multilayer PC-based mirror made of high- and low-index oxide layers. In this design, the incoming light is mostly reflected back onto the photoactive layer within a broad spectral range, and only a narrow portion passes through the design. This leads to the simultaneous realization of high-power conversion efficiency of 10.12%, and the generation of semitransparent colors. The portion of reflected/transmitted Vis light can easily be controlled by scanning the angle of light incidence; this, in turn, arises from the angle sensitivity of the PC-based mirror [79].

Considering all of the aforementioned discussions, optical interference could be vitally important to the design of future PV cells, where bringing the active-layer thickness to a level as thin as the carrier's

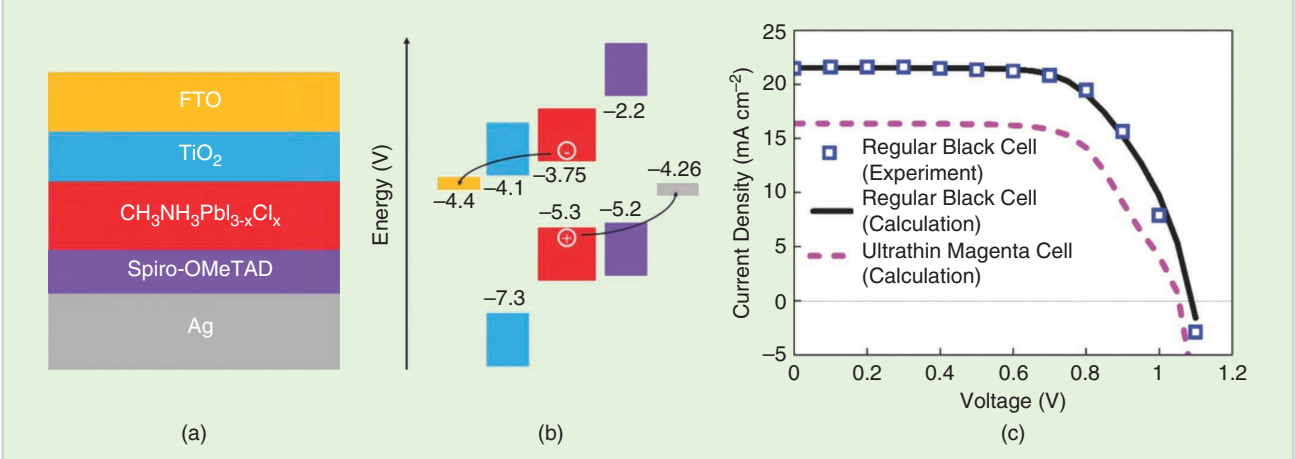

FIGURE 4 (a) The proposed colored, perovskite-based solar cell design with its corresponding (b) band alignments and (c) J-V characteristics. (Used with permission from [75].) FTO: fluorine-doped tin oxide; $CH_3NH_3PbI_3$-xClx: perovskite active layer; Spiro-OMeTAD: hole transport layer.

diffusion length, enables us to fabricate moderate-to-high efficiency solar cells with common and low-cost fabrication routes. Consequently, this makes further upscaling possible for practical and large-scale applications. These ideas may also be employed for emission applications. As previously indicated, strong interference in the semiconductor layers is generally achieved in nanometer-scale dimensions. On the other side, shrinking the semiconductor nanoparticles' dimension down to their exitonic Bohr radius can significantly enhance their emission capabilities [80]–[82]. As a result, transferring an ultrathin layer made of luminescent colloidal particles into a predesigned optical cavity can significantly enhance their photoluminescence.

PHOTOELECTROCHEMICAL WATER SPLITTING

Another field that has attracted recent attention is photoelectrochemical water splitting (PEC-WS). During this process, a basic cell is made of at least one semiconductor as a photoanode or photocathode and a metal (which is commonly platinum) as a counter electrode. Upon shining the photoelectrode design, electron-hole pairs are generated. These pairs are spatially separated in semiconductor-electrolyte and semiconductor-semiconductor interfaces. Afterward, electrons travel toward the external circuit through electron transport layers and generate hydrogen (H_2) in the counter electrode. On the other side, holes move toward the semiconductor-electrolyte interface to contribute to water oxidation. Therefore, similar to PV cells, minimizing the carrier's diffusion length by reducing the active-layer thickness is an efficient way to increase the photoactivity of the photoelectrode.

Unlike PV cells, which generally need three layers of electron transport, layer-absorbing, layer-hole transport layers, PEC-WS cells operate using a single semiconductor layer in which the charge separation in the semiconductor-electrolyte interface is achieved by an external bias. As a result, using MS or MOS simple-resonant designs for high-activity PEC-WS cells seems promising. It was proven that using proper configuration and material thickness leads to broadband light absorption in different semiconductors.

> By tuning the oxide- and semiconductor-layer thickness, the spectral position of the absorption peak can be tuned.

For example, in high-index semiconductors such as Ge or MoS_2, this broadband absorption is achieved in thin-layer thicknesses (below 10 nm) using MOS cavity designs [1]. For semiconductors with a lower refractive index and an extinction coefficient, e.g., metal oxides or organic semiconductors, these matching conditions are satisfied in coatings greater than 20-nm-thick by an MS cavity structure. One of the most commonly utilized metal oxides for PEC-WS is hematite (α-Fe_2O_3), which is due to its narrow band gap that extends its absorption toward the Vis range. However, its PEC-WS performance is mainly limited by its poor electrical properties, i.e., having a hole-diffusion length fewer than 16 nm [83]. Therefore, the photogenerated carriers within the bulk (more than 16 nm away from the surface) cannot be effectively collected. An efficient design should be able to harvest light in thicknesses close to this hole-diffusion length. A 22-nm-thick Fe_2O_3 on Ag-reflecting thickness has been demonstrated to show a near-unity absorption at $\lambda < 450$ nm [51].

In one of the earliest uses of resonant planar designs for PEC-WS, Dotan et al. proposed a cavity design that enhances light absorption in a thin α-Fe_2O_3 layer. Introducing this design strategy, an average above band gap absorption of 71% was accomplished in an active-layer thickness of 50 nm [84]. In another study, a 25-nm-thick α-Fe_2O_3 was synthesized using atomic layer deposition (ALD) on a Pt mirror capped with a thin TiO_2 protection layer, representing both high chemical stability and PEC-WS activity [85]. This design strategy was employed for other similar configurations, such as an Au-Fe_2O_3 heterostructure [86]. With this MS design, the formation of Fabry–Perot (FP) resonance between the layers causes light absorption within both layers. Thus, the existence of parasitic absorption within the bottom metal layer limits the amount of absorption inside the photoactive semiconductor layer. To mitigate this deficiency, a lossless dielectric-based PC mirror was employed to maximize light absorption in the semiconductor layer [87].

In this article, to further boost device performance, two cells were fabricated and placed face to face to increase the optical path of the light within the cavity and to harvest all the incoming light. To substantiate the activity of the design, electrical properties of the cell have also been improved through the use of a cocatalyst, which expedites the carrier dynamics in a semiconductor-electrolyte interface.

Another promising low-band MOS is Bi vanadate ($BiVO_4$). For this semiconductor, the use of a MOS cavity design proved to be an efficient approach that significantly enhances the activity of the design compared to that of a bare layer. This MOS cavity design was subsequently transferred to the top of a pre-patterned polydimethylsiloxane (PDMS) scaffold. The combination of FP cavity modes and diffraction-assisted light trapping further increased the efficiency of the WS cell [88]; [see Figure 5(a) and (b)]. Figure 5(c) and (d) includes a textured $BiVO_4$ photoelectrode improves the photocurrent value from 0.34 mA cm^{-1} at 1.23 $V_{\text{reversible hydrogen electrode}}$ (V_{RHE}) (for a $SnO_2/BiVO_4$-thin film), to 0.86 (for $Au/SnO_2/BiVO_4$ on a flat substrate) and 1.37 mA cm^{-1} (for $Au/SnO_2/BiVO_4$ on a patterned PDMS) and further, to 2 mA cm^{-1} at 1.23 V_{RHE} when an iron oxyhydroxide oxygen-evolution catalyst was added (for $Au/SnO_2/BiVO_4$ + goethite (FeOOH) on a patterned PDMS).

Although the aforementioned discussions prove the functionality of MOS and MS designs for ultrathin PEC-WS, there remains a synthetic challenge that must be addressed. Most chemically synthesized metal oxides require a post-annealing process that refines their crystallinity and increases their electron mobility via a reduction in trap-state densities and grain boundaries. For instance, the common annealing temperature for an α-Fe_2O_3 layer is roughly 800 °C, which is close to the melting point of most reflecting noble metals. Considering that the fabrication steps of a cavity starts with the deposition of a bottom metal mirror, the annealing step is applied for both metals; this, in turn, hampers the specular reflectivity of the design. Thus, the overall optical performance of the cavity is disturbed.

It is essential to develop a transfer technique that isolates the bottom layers from the annealing process. Recently, Kay et al. developed a film flip and transfer process to make the coating of the metal layer after the annealing step [89], as shown in Figure 6(a). In addition to improving the electrical properties of the layer, the layer is homogeneously doped using Ti. Although theoretical results estimated the highest absorption in a 20-nm-thick semiconductor layer, the highest photocurrent values were obtained for an 8-nm-thick layer, as demonstrated in Figure 6(b). It was assumed that this was because the short diffusion length of holes where the generated carriers within the bulk of the layer were recombined before they reached the surface. The activity was gradually enhanced by adding a cocatalyst into the system. Finally, the author employed a heterogeneous doping with the 1 catalyst percentage (cat%) zinc (Zn)—undoped—1 cat% Ti to maximize the response. As shown in Figure 6(c), this modification led to a 1.01-mA cm^{-2} photocurrent in the reversible water oxidation potential (1.23 V versus RHE) for a 14-nm-thick active layer.

The spalling process is another synthesis approach that creates metal-backed, single-crystalline, ultrathin semiconductor layers. Using Si and gallium arsenide

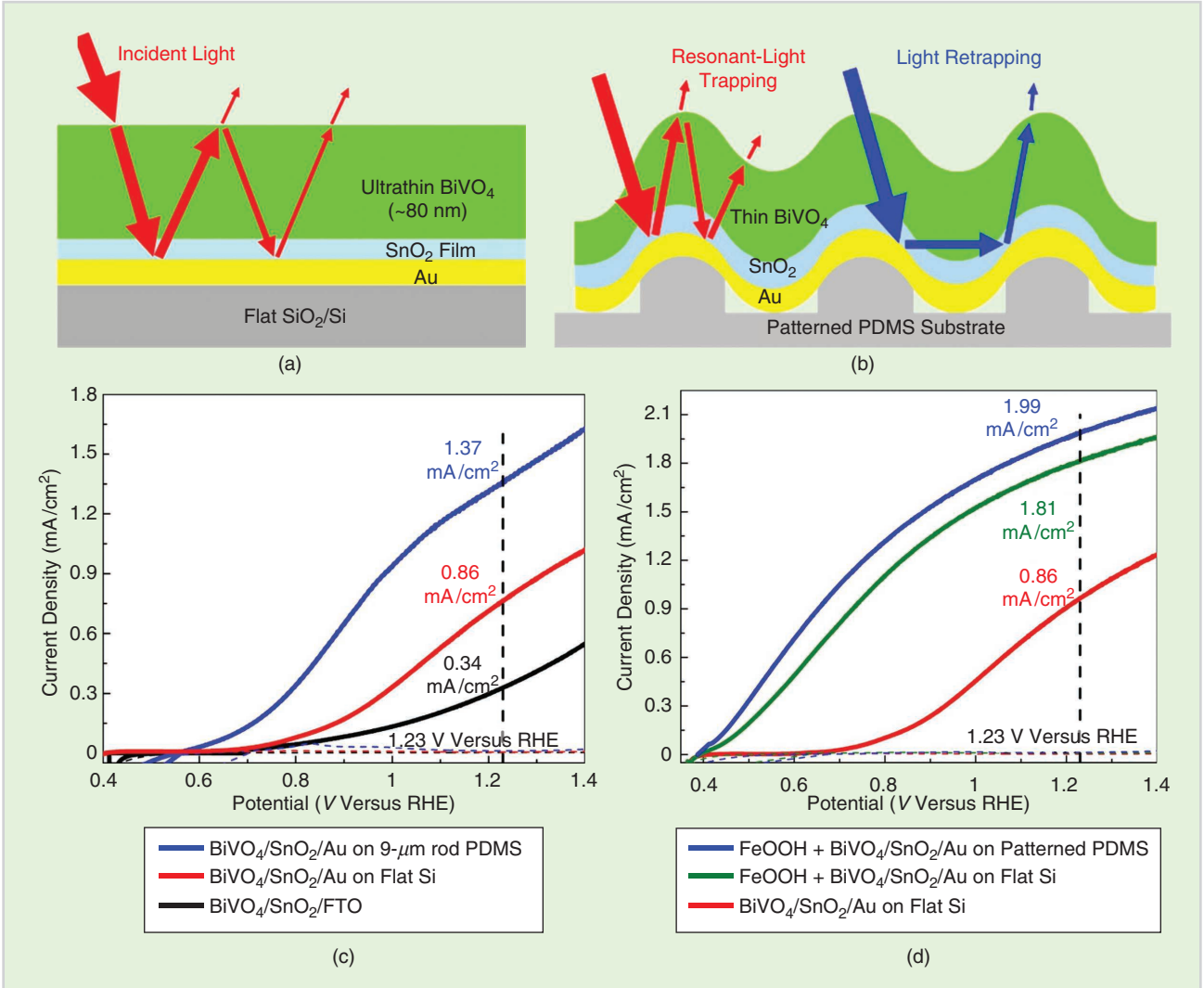

FIGURE 5 The proposed MIS cavity on (a) a flat and (b) a textured design. (c) The linear sweep voltammetry of different configurations and (d) their responses upon adding a catalyst on top of the active $BiVO_4$ layer. (Used with permission from [88].) PDMS: polydimethylsiloxane; FeOOH: goethite; RHE: reversible hydrogen electrode.

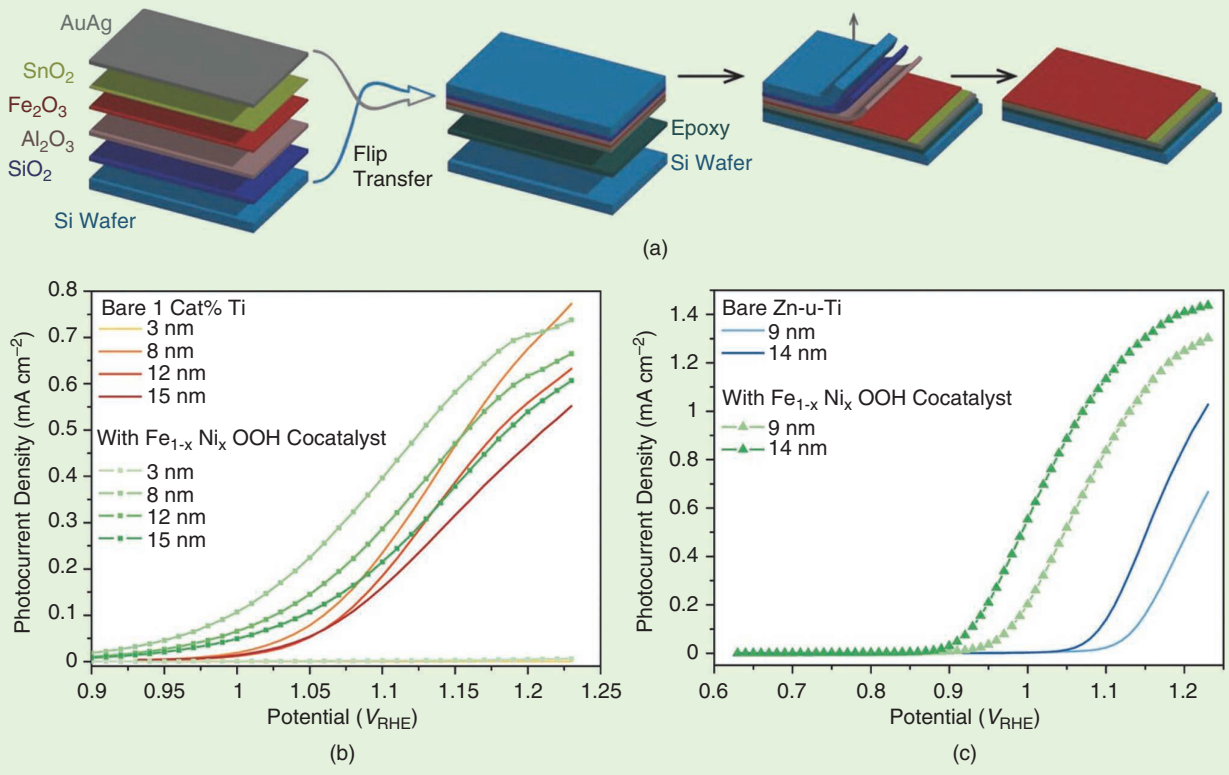

FIGURE 6 (a) The fabrication route used to synthesize an α-Fe_2O_3-based MOS cavity, (b) the photocurrent values of the photoanode for different semiconductor-layer thicknesses, and (c) the doping conditions. (Used with permission from [89].) $Fe_{1-x}NI_xOOH$: co-catalyst; Zn-u-Ti: Zn-doped–undoped-Ti-doped.

as single-crystalline, high-mobility semiconductors in MS configurations offers a high-efficiency photocathode [90].

In addition to semiconductor-based WS cells, utilizing hot, electron-based designs has garnered much attention for obtaining highly stable, metal-based photoanodes [91]. Shi et al. proposed an MIM cavity made of Au mirror/TiO_2/Au nanoparticles as photoanodes for water oxidation [92]. This design configuration shows strong modal coupling between the FP cavity modes of the Au mirror/TiO_2 and localized surface plasmon resonance of the Au nanoparticles. Figure 7(a) and (b) illustrates the proper choice of spacer and top-layer thickness leads to a black light absorber. The existence of strong interference—as a result of inserting the Au mirror—leads to an 11-fold enhancement in the incidence of photon-to-current conversion efficiency compared to designs without the cavity.

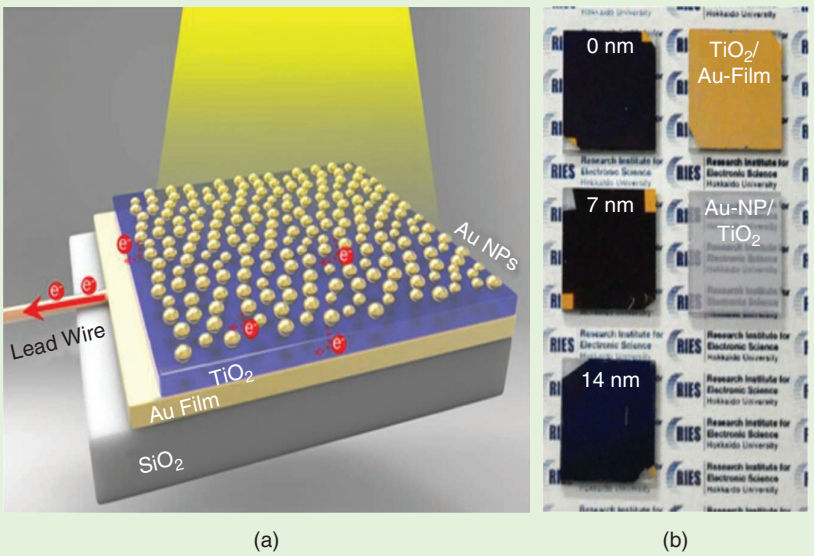

FIGURE 7 (a) A schematic of the proposed MSM cavity with partially inlaid Au nanoparticles. (b) Photos of Au nanoparticle/TiO_2/Au film structures with inlaid depths of 0, 7, and 14 nm, respectively. Photos of the 2-nm TiO_2/Au film structure without Au nanoparticles and the Au NP/28-nm TiO_2 structure without Au film are shown for comparison. (Used with permission from [92].) NP: nanoparticle.

The spalling process is another synthesis approach that creates metal-backed, single-crystalline, ultrathin semiconductor layers.

Similar studies were also performed in which the top nanounit surface was achieved using the dewetting process [93], [94]. During the dewetting process, a thin metal layer is annealed at a temperature close to its melting point, which transforms it into a nanoisland layer. In the MIM designs mentioned previously, incoming light is coupled into the nanostructured top layer and generates hot electrons. These hot electrons are separated using a TiO_2 transport layer and are transferred toward the rear metal contact. The left hot holes undergo a water-oxidation reaction to split water to oxygen. As discussed previously, the spacer layer is a lossless medium with no absorption characteristics in the Vis range.

Recently, the concept of gap plasmon resonances was introduced in an MSM architecture. In this design, the bottom mirror was Au or Pt, the middle semiconductor was a 50-nm-thick Vis-absorbing WO_3, and the top layer was dewetted Au nanoparticles [95]. This design obtained its response simultaneously from the top plasmonic layer and middle semiconductor spacer. The formation of gap plasmon polaritons confine light within the semiconductor bulk underneath the top Au nanoislands. This confined field is harvested in both metal and semiconductor layers. Moreover, the strong interference between the bottom mirror and lossy semiconductor layer leads to strong absorption in both the top metal and spacer. All of the previously discussed studies demonstrate tremendous potential for lithography-free semiconductors and plasmonic, metal-based, perfect absorbers for PEC-WS application.

FILTERING

Another application that can be implemented using these strong-interference, multilayer absorbers is filtering. The selective absorption of a portion of the EM spectrum in the Vis range leads to the formation of color filters. As previously indicated, cavity designs composed of MI pairs with a noble metal such as Au or Ag, have narrow spectral absorption. The most common type of these cavities is MIM. In an MIM configuration, the formation of FP resonances leads to light-perfect absorption in a narrow spectral range. Based on the thickness of the bottom metal layer, MIM cavities can act as both transmittive and reflective color filters. If the bottom metal layer is thick, the structure operates as a reflective color filter that absorbs a narrow range and reflects the rest of the spectrum. By adopting the insulator-layer thicknesses, three distinctive colors of cyan, magenta, and yellow can be generated from the incidences of white light. However, if the bottom metal is thin, the structure acts as a transmittive color filter with RGB colors in the output, as shown in Figure 8(a)–(c). The planar nature of these FP-based color filters makes them excellent choices for large-scale applications [96].

Several different MI pair combinations have been employed to obtain high-efficiency color filters [19], [20], [22], [43], [97]. One of the main challenges of these MIM color filters is their angle-sensitive response. Considering that these designs work based on the interference between reflected and transmitted waves, as we increase the angle of incidence, the optical path of the light increases, which subsequently leads to a red shift in the spectrum. This can be decrease by using high-index, dielectric insulator spacers, e.g., Si nitride [98], Zn sulfide [42], WO_3 [39], and TiO_2 [19], [29], [41]. Based on Snell's law, as

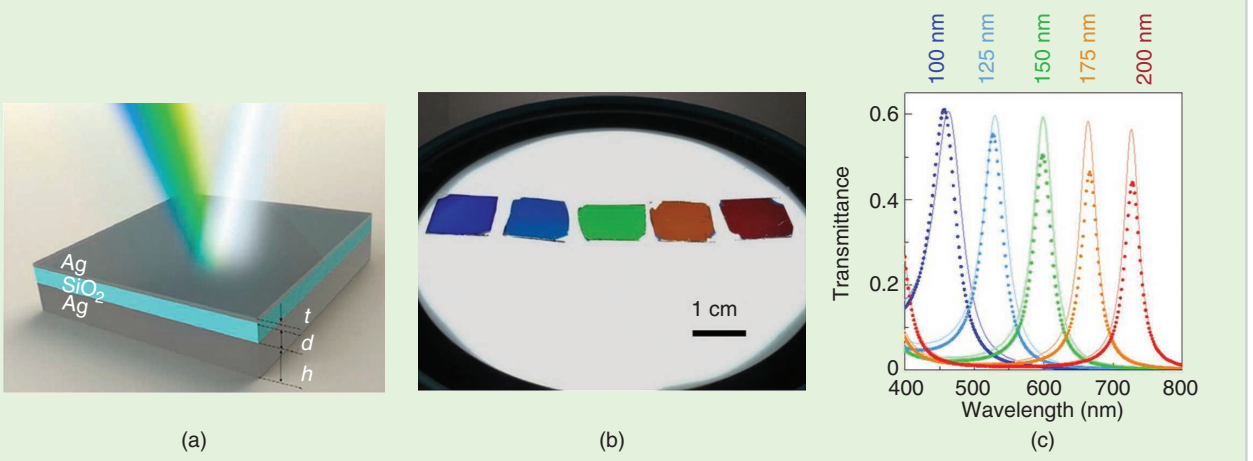

FIGURE 8 (a) The proposed MIM-based color filter composed of Ag-SiO_2-Ag, (b) the optical image of fabricated color filters, and (c) the transmission response of these filters with different spacer thicknesses. (Used with permission from [96].)

we increase the insulator layer's refractive index, the refracted wave approaches normal incident, and consequently, the optical path difference for different incident angles decreases [99].

Another solution for this problem is to place an overlay on top of the cavity [17]. This sensitivity can be significantly suppressed in high-index, semiconductor-based cavity designs. It has been proven that MS junctions with the proper materials and dimensions are an efficient way to fabricate angle-insensitive color filters [38], [40], [100]. The main issue with these MS color filters is their poor color purity; generally, these type of color filters have a broader resonance response, which increases the crosstalk and reduces the generated color's pureness.

Another drawback with these color filters is their inefficiency, which is more pronounced in the transmissive color filters that generate RGB colors. In these designs, light passes through multiple metal and insulator layers and due to the inherent loss of these layers, RGB color-generation efficiency is limited to values as small as ~0.6. RGB colors with high efficiency can be created using plasmonic and guided-mode, resonance-based designs [101]–[113]. However, these designs have complex, large-scale, incompatible fabrication routes. Moreover, because of the geometrical asymmetry of resonant nanounits such as gratings, they can efficiently operate in specific polarization, and their response is completely gone in other polarizations. Taking the unpolarized nature of sun irradiation into account as well as the large-scale incompatibility of the EBL process, these plasmonic-based color filters are improper designs for practical use. Thus, an innovative architecture should be developed to achieve high-efficiency RGB colors using FP-based designs.

Yang et al. proposed the use of lossy-absorbing, nickel-based MIM cavities to obtain additive colors in the reflection mode [114], as included in Figure 9(a)–(c). In this case, the MIM structure absorbs most of the Vis light and reflects a narrow range in the reflection output. Using a multithickness oxide layer, a spatially variant color filter can be achieved [Figure 9(d)]. Moreover, the proposed design shows a small, ultimate resolution for color printing [Figure 9(e)]. Although the proposed design demonstrated high reflection efficiency, it suffered from poor color purity.

Recently, we proposed an elegant design made of MIMI–semiconductor (MIMIS) configurations [115]. This cavity design is a series combination of MIM MIS cavities. The bottom MIM cavity absorbs the large wavelength values, while the top MIS structure is active in the shorter wavelengths; therefore, only the middle spectral portion is reflected in the output. Utilizing this MIMIS architecture, RGB colors were generated with high color purity and high efficiency (i.e., as high as 0.7). Aluminum (Al) and Ge were used as the metal and semiconductor layers, respectively. To reduce the angle

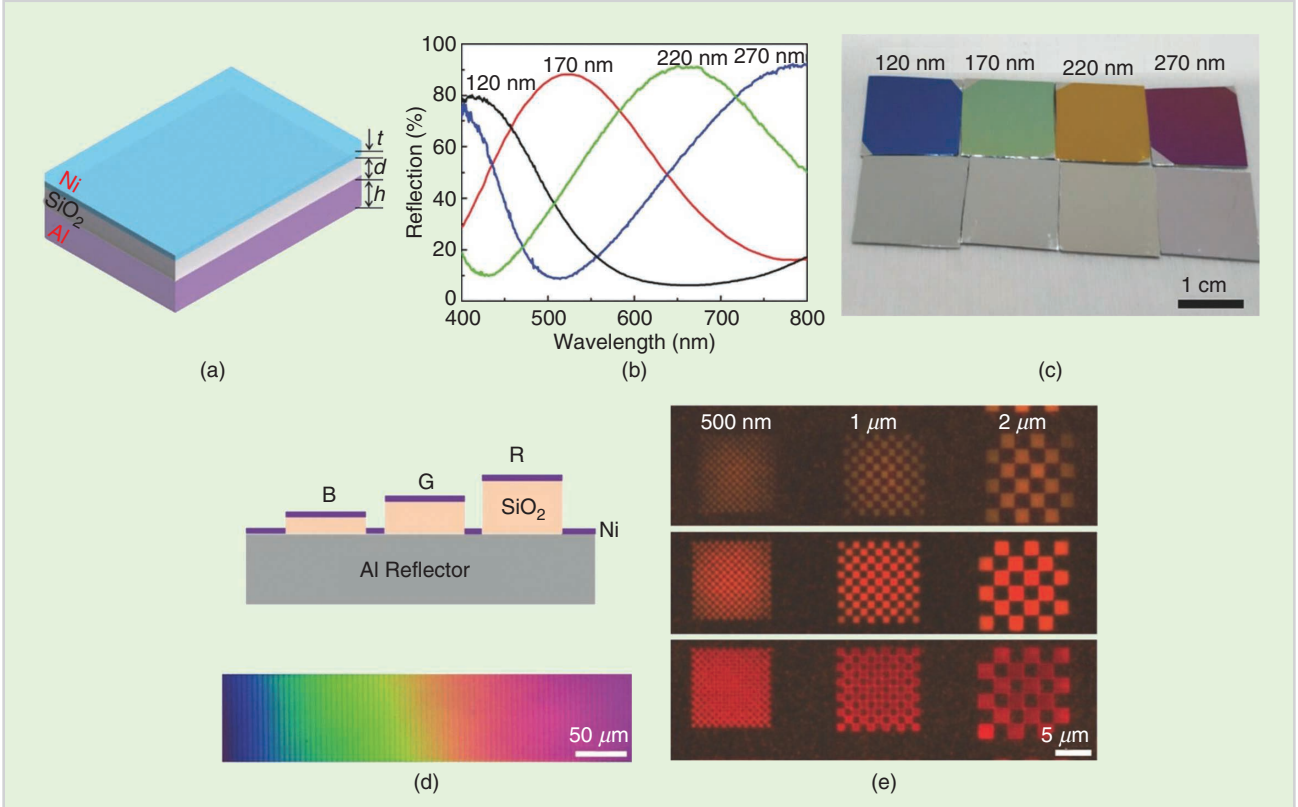

FIGURE 9 (a) The lossy, nickel (Ni)-based, MIM color filter, (b) the measurement results of its reflection for four different insulator-layer thicknesses, (c) the optical image of the fabricated color filters (the bottom samples are MI pairs without an Ni top layer), (d) the fabrication of spatially variant color filters with tuning of the SiO_2-layer thickness, and (e) colorful checkerboard patterns with different sizes, which show the ultimate resolution of FP cavity, color-based filters for color printing. (Used with permission from [114].) B: blue; G: green; R: red.

sensitivity of the absorption response, ZnO with a refractive index of 1.9 was applied as an insulator layer. We further improved RGB color-generation efficiency by employing a Bi-based MIMI filter [46]. It was theoretically and experimentally shown that the structure composed of Al-LiF-Bi-LiF layers can create additive RGB colors with an amplitude as large as 0.9.

SENSING

Sensing is another potential application of these planar-perfect absorbers. As mentioned previously, a multilayer structure exhibits resonant behavior at a specific frequency. This can be seen as a dip in reflection or a peak in the absorption spectra. The resonance spectrally shifts when it interacts with external stimuli. The amount of resonance peak shift depends on the refractive index of the surrounding medium, and this, in turn, can be used to understand the type of stimuli. A planar multilayer sensor has a polarization-insensitive response, which makes it a suitable option for practical use.

One of the most common design architectures for biosensing is prism-coupled surface plasmon resonance. Although this structure is a planar multilayer design, to excite surface plasmon polaritons, we must couple a 3D prism with this design. In this article, we therefore omit these sensing schemes because our main goal is to propose sensing schemes in simple planar designs.

Sreekanth et al. experimentally realized the point of darkness and singular phase by employing an asymmetrical, MI pair-based stack [116]. At a specific wavelength and angle of incidence, the incoming p-polarized light experiences a near-zero reflection (i.e., point of darkness). Here, the stack undergoes an abrupt phase change because of the existence of a highly absorbent ultrathin film, which in this case is Ge. To verify its biosensing behavior, the top surface is functionalized with a thin, thiolated biotin that captures streptavidin. The design shows enhanced phase sensitivity for streptavidin concentrations as low as 1 picomolar. The calculated figure of merit for this multilayer stack was 445. If the operational wavelength of the sensor is located within the Vis regime, then a colorimetric-detection scheme can be realized. In this case, the change in color can be used to predict the object. A simple MS junction composed of Al and 20-nm-thick Si as the metal and top layers, respectively, was demonstrated as a colorimetric biosensor. The deposition of an ultrathin dielectric layer on top of its surface causes a red shift in the resonance frequency. The biosensing functionality of this MS resonator is examined by bovine serum albumin molecules, as shown in Figure 10(a)–(d). With its planar nature and operational frequency (which is located inside the Vis spectrum), this biosensor offers a robust way to determine the bioagent type using only the naked eye [117].

Serhatlioglu et al. demonstrated an H_2 sensor based on a quarter-wavelength MIM cavity design. In this design, 7-nm-thick palladium (Pd) was chosen as the top layer. Pd has dual functionality: 1) as a lossy metal that provides light-perfect absorption in the resonance frequency of the cavity and 2) as an H_2 catalyst that transforms into palladium hydride (PdH_x) when exposed to H_2 gas. The proposed MIM resonator has a reflection dip in the Vis range. As PdH_x is formed, the effective permittivity of the top layer changes, imposing a red shift in its dip-spectral position [118]. This colorimetric diagnostic can be achieved by using SPR-based structures.

A three-layered Ag nanoparticles-based sheet deposited on top of an Au substrate was synthesized via the Langmuir–Schaefer route [119]. The binding of an avidin-biotin bioagent caused a drastic change in the sample's color, thus making biosensing possible using only the naked eye. A single layer of Au nanoparticles can be also utilized to produce a label-free biosensor on a chip. The sensitivity of the design was shown to be in direct correlation with the particle size. Au nanoparticles with different sizes of 12–48 nm were chemisorbed on top of amine-functionalized glass. Sensors with a 39-nm-diameter Au nanoparticles revealed maximum sensitivity [120].

To excite SPR using a lithography-free fabrication route, several nonchemical

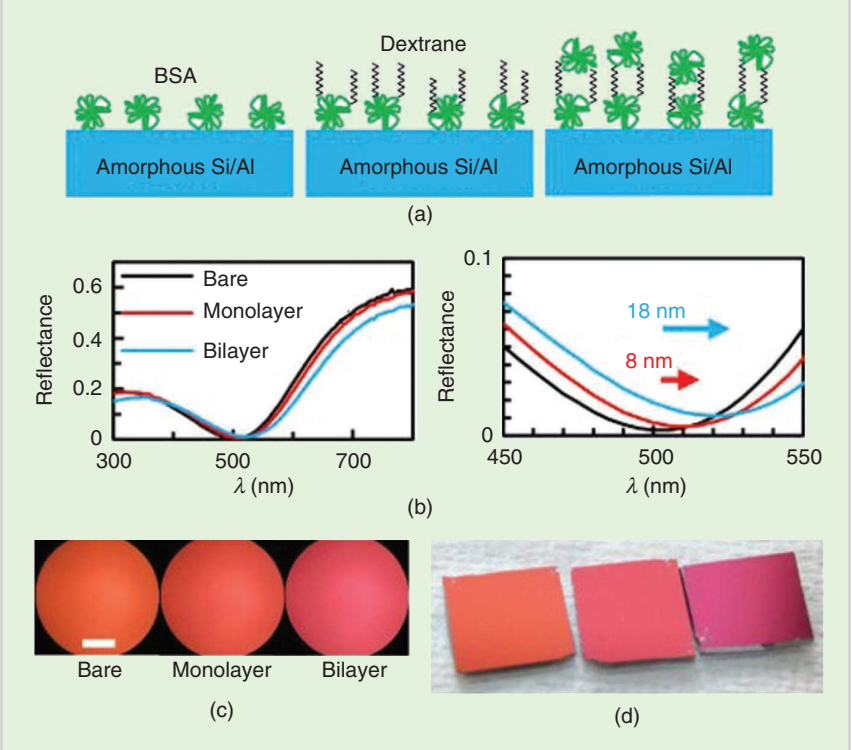

FIGURE 10 (a) A schematic representation of the monolayer and bilayer bovine serum albumin (BSA) synthesis on top of the MS design. (b) A measured reflectance response of the design with and without monolayer and bilayer protein molecules. (c) An optical image of the samples. (d) A photo of the samples under ambient light. (Used with permission from [117].)

synthesis approaches, such as dewetting, can be followed. Depending on the layer thickness, annealing temperature, and metal type, the particle's size and distribution can be tuned in a practical way. It is in this way that we can realize resonant designs in the Vis range. Morphology control of the dewetted film can be enhanced by double-step growth of nanoislands [121]. The dewetted films can be also utilized as a nanomasking layer to create nanostructures via a lithography-free route. It was shown that Si and Si-SiO_2 nanostructures capped with an Au particle can provide a colorimetric-detection scheme with a sensitivity of 70.8 nm refractive index unit^{-1} which was roughly two-times larger than that of periodically patterned designs using the lithography technique [122]. As a result, these random nanoparticles are not only easy to obtain, they also achieve a better sensing performance.

Other innovative, lithography-free design architectures have been proposed for sensing applications [123], [124]. Recently, an ultrathin TiO_2 on top of an MI cavity was proved to photo catalytically reduce carbon dioxide. The proposed cavity provides strong light absorption in ultrathin, TiO_2-layer thicknesses of 2 nm. As depicted in Figure 11(a)–(e), the as-obtained structures significantly improve TiO_2-photocatalytic activity and selectivity of oxygenated hydrocarbons more so than does the benchmark photocatalyst (Aeroxide P25). Remarkably, the MIS cavity results in hydrocarbon formation rates of 0.967 mmol $g^{-1}h^{-1}$, corresponding to 1,145-times higher activity than Aeroxide P25 [125].

CONCLUSION AND FUTURE DIRECTIONS

In this article, we showed how strongly interacting, lithography-free, photoelectronic devices can be realized with high-operational performance in the Vis and NIR regimes. These planar-perfect absorbers can be made of metals or semiconductors. In the case of metal-based perfect absorbers, the absorption BW could cover narrow or broad spectral ranges. The narrow response of these metal-based cavities has direct application in the design of Vis light filters. Moreover, their integration into solar cell

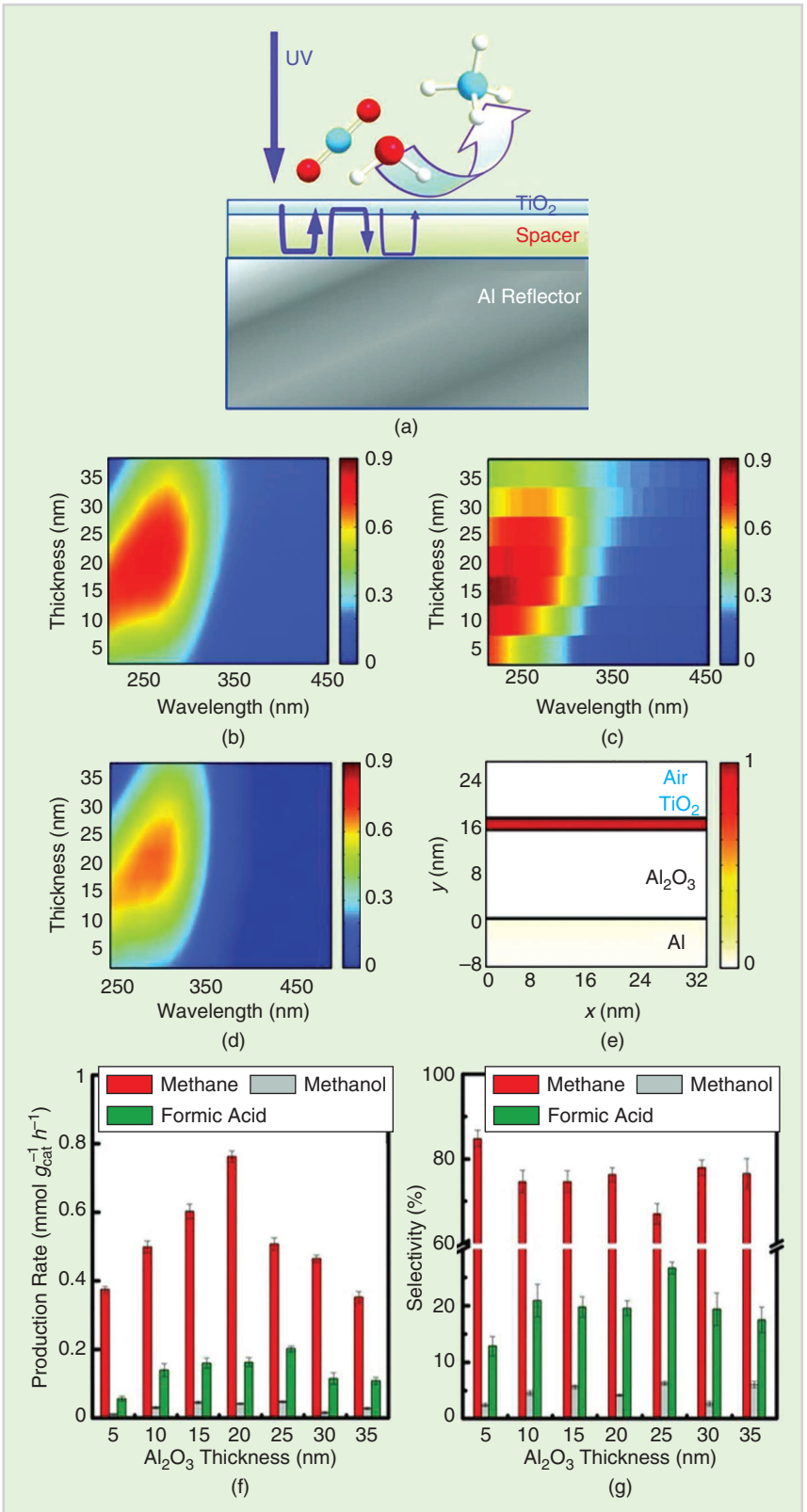

FIGURE 11 (a) The proposed three-layered, MIS perfect absorber, (b) measured absorption, and (c) the modeled absorption spectra of Al/Al_2O_3/2-nm TiO_2 as a function of Al_2O_3 thickness. (d) Modeled exclusive absorption in the TiO_2 layer as a function of TiO_2 thickness. (e) Modeled exclusive absorption in the 2-nm-thick TiO_2 layer on the 15-nm Al_2O_3/Al cavity, (f) the output product, and (g) the corresponding selectivity. (Used with permission from [125].) UV: ultraviolet; Al_2O_3: aluminum oxide.

To excite SPR using a lithography-free fabrication route, several nonchemical synthesis approaches, such as dewetting, can be followed.

designs provides an opportunity to create colorful and decorative solar cells with a moderately high performance.

Narrow-band absorbers may also be used for gas sensing, e.g., with H_2 gas. In this case, exposing the cavity to H_2 gas changes the dielectric function of metal, and consequently, a shift is recorded in the resonance wavelength. In the other side, the broadband absorbers are of particular interest for photo-conversion applications such as PVs and PEC-WS. The excitation of plasmonics and generation of hot electrons in the broad spectral regime can be used to acquire highly efficient and stable, photo electronic devices. Note that another common application of metal-based perfect absorbers is thermal PVs.

In this article, however, we mainly focused on the Vis and NIR regimes, and the operation of perfect absorbers in this range was investigated. Semiconductors can also support strong interference effects in ultrathin dimensions; however, the difference is their operational spectrum range. Semiconductors can only absorb photons with energies above their optical band gap; therefore, their perfect absorption BW is limited to Vis and short, NIR ranges. For semiconductor-based optical devices, narrow-band absorption responses can be used to realize color filters or spectrally selective photodetectors. Additionally, strong interference in ultrathin cavity designs can be modulated with an external biosensing agent; thus, a biosensor can be made using these semiconductor-based cavities.

On the other hand, the use of proper configurations and geometries can lead to light absorption in a broad frequency range. This will be beneficiary for PVs and PEC-WS applications, where a higher-absorption BW causes larger photocarrier density, resulting in enhanced design photoconversion efficiency.

All of these design architectures have simple, large-scale, compatible fabrication routes that make them excellent choices for future upscaling. With respect to photoconversion devices, a further performance enhancement of the design can be accomplished by introducing high-crystalline, high-mobility, ultrathin semiconductors. For filtering applications, in addition to searching for new low-loss materials, innovative design architectures such as multicavity designs can further enhance color purity and efficiency. These strong interferences, together with polarization insensitivity characteristics, could also enable sensing in the visible range using the naked eye. The proposed designs can provide a robust method for obtaining practical diagnostic systems.

ABOUT THE AUTHORS

Amir Ghobadi (amir@ee.bilkent.edu.tr) is with the Department of Electrical and Electronics Engineering, Bilkent University, Ankara, Turkey.

Hodjat Hajian (hodjat.hajian@bilkent.edu.tr) is with the Nanotechnology Research Center, Bilkent University, Ankara, Turkey.

Bayram Butun (bbtn@bilkent.edu.tr) is with the Nanotechnology Research Center, Bilkent University, Ankara, Turkey.

Ekmel Ozbay (ozbay@bilkent.edu.tr) is with the Nanotechnology Research Center, the Department of Electrical and Electronics Engineering, the Department of Physics, and the UNAM-Institute of Materials Science and Nanotechnology, Bilkent University, Ankara, Turkey.

REFERENCES

[1] A. Ghobadi, H. Hajian, B. Butun, and E. Ozbay, "Strong light—Matter interaction in lithography-free planar metamaterial perfect absorbers," *ACS Photon.*, vol. 5, no. 11, pp. 4203–4221, 2018.

[2] X. Liu, T. Starr, A. F. Starr, and W. J. Padilla, "Infrared spatial and frequency selective metamaterial with near-unity absorbance," *Phys. Rev. Lett.*, vol. 104, no. 20, p. 207403, 2010.

[3] H. Wang and L. Wang, "Perfect selective metamaterial solar absorbers," *Opt. Exp.*, vol. 21, S6, pp. 13,311–13,319, 2013.

[4] M. G. Nielsen, A. Pors, O. Albrektsen, and S. I. Bozhevolnyi, "Efficient absorption of visible radiation by gap plasmon resonators," *Opt. Exp.*, vol. 20, no. 12, pp. 13,311–13,319, 2012.

[5] X. Ming and Q. Tan, "Design method of a broadband wide-angle plasmonic absorber in the visible range," *Plasmonics*, vol. 12, no. 1, pp. 14–17, 2017.

[6] K. Aydin, V. E. Ferry, R. M. Briggs, and H. A. Atwater, "Broadband polarization-independent resonant light absorption using ultrathin plasmonic super absorbers," *Nat. Commun.*, vol. 2, p. 517, Nov. 2011.

[7] M. Kenney, J. Grant, Y. D. Shah, I. Escorcia-Carranza, M. Humphreys, and D. R. S. Cumming, "Octave-spanning broadband absorption of terahertz light using metasurface fractal-cross absorbers," *ACS Photon.*, vol. 4, no. 10, pp. 2604–2612, 2017.

[8] X. Duan, S. Chen, W. Liu, H. Cheng, and Z. Li, "Polarization-insensitive and wide-angle broadband nearly perfect absorber by tunable planar metamaterials in the visible regime," *J. Opt.*, vol. 16, no. 12, p. 125,107, 2014.

[9] A. K. Azad et al., "Metasurface broadband solar absorber," *Sci. Rep.*, vol. 6, p. 20,347, Feb. 2016.

[10] R. Mudachathi and T. Tanaka, "Broadband plasmonic perfect light absorber in the visible spectrum for solar cell applications," *Adv. Nat. Sci. Nanosci. Nanotechnol.*, vol. 9, p. 015,010, Feb. 2018.

[11] Y. Lu, W. Dong, Z. Chen, A. Pors, Z. Wang, and S. I. Bozhevolnyi, "Gap-plasmon based broadband absorbers for enhanced hot-electron and photocurrent generation," *Sci. Rep.*, vol. 6, p. 30,650, July 2016.

[12] G. Tagliabue, H. Eghlidi, and D. Poulikakos, "Facile multifunctional plasmonic sunlight harvesting with tapered triangle nanopatterning of thin films," *Nanoscale*, vol. 5, no. 20, pp. 9957–9962, 2013.

[13] A. Ghobadi et al., "Visible light nearly perfect absorber: An optimum unit cell arrangement for near absolute polarization insensitivity," *Opt. Exp.*, vol. 25, no. 22, p. 27,624, 2017.

[14] T. Ji, Y. Wang, Y. Cui, Y. Lin, Y. Hao, and D. Li, "Flexible broadband plasmonic absorber on moth-eye substrate," *Mater. Today Energy*, vol. 5, pp. 181–186, Sept. 2017.

[15] J. A. Bossard, L. Lin, S. Yun, L. Liu, D. H. Werner, and T. S. Mayer, "Near-ideal optical metamaterial absorbers with super-octave bandwidth," *ACS Nano*, vol. 8, no. 2, pp. 1517–1524, 2014.

[16] F. Ding, J. Dai, Y. Chen, J. Zhu, Y. Jin, and S. I. Bozhevolnyi, "Broadband near-infrared metamaterial absorbers utilizing highly lossy metals," *Sci. Rep.*, vol. 6, p. 39,445, Dec. 2016.

[17] C. S. Park, V. R. Shrestha, S. S. Lee, and D. Y. Choi, "Trans-reflective color filters based on a phase compensated etalon enabling adjustable color saturation," *Sci. Rep.*, vol. 6, p. 25,496, May 2016.

[18] K. Mao et al., "Angle insensitive color filters in transmission covering the visible region," *Sci. Rep.*, vol. 6, p. 19,289, Jan. 2016.

[19] Y.-T. Yoon and S.-S. Lee, "Transmission type color filter incorporating a silver film based etalon," *Opt. Exp.*, vol. 18, no. 5, pp. 5344–5349, 2010.

[20] D. Zhao et al., "Ultra-narrow-band light dissipation by a stack of lamellar silver and alumina," *Appl. Phys. Lett.*, vol. 104, no. 22, p. 221,107, 2014.

[21] J. Y. Lee, K. T. Lee, S. Seo, and L. J. Guo, "Decorative power generating panels creating angle insensitive transmissive colors," *Sci. Rep.*, vol. 4, p. 4192, Feb. 2014.

[22] S. S. Mirshafieyan and D. A. Gregory, "Electrically tunable perfect light absorbers as color filters and modulators," *Sci. Rep.*, vol. 2635, pp. 1–9, Jan. 2018. doi: 10.1038/s41598-018-20879-z.

[23] H. A. O. P. Eng, Y. I. L. Uo, X. I. Y. Ing, Y. P. U. Ang, Y. A. J. Iang, and J. X. U. Immy, "Broadband and highly absorbing multilayer structure in mid-infrared," *Appl. Opt.*, vol. 55, no. 31, pp. 8833–8838, 2016.

[24] Z. Li, E. Palacios, S. Butun, H. Kocer, and K. Aydin, "Omnidirectional, broadband light absorption using large-area, ultrathin lossy metallic film coatings," *Sci. Rep.*, vol. 5, p. 15,137, Oct. 2015.

[25] A. Ghobadi, S. A. Dereshgi, B. Butun, and E. Ozbay, "Ultra-broadband asymmetric light transmission and absorption through the use of metal free multilayer capped dielectric microsphere resonator," *Sci. Rep.*, vol. 7, p. 14,538, Nov. 2017.

[26] N. Mattiucci, M. J. Bloemer, N. Akozbek, and G. D'Aguanno, "Impedance matched thin metamaterials make metals absorbing," *Sci. Rep.*, vol. 3, pp. 1–11, Nov. 2013, doi: 10.1038/srep03203, [Online]. Available: https://www.nature.com/articles/srep03203

[27] M. Chirumamilla et al., "Multilayer tungsten-alumina-based broadband light absorbers for high-temperature applications," *Opt. Mater. Exp.*, vol. 6, no. 8, p. 2704, 2016.

[28] H. Deng, Z. Li, L. Stan, D. Rosenmann, and D. Czaplewski, "Broadband perfect absorber based on one ultrathin layer of refractory metal," *Opt. Lett.*, vol. 40, no. 11, pp. 2592–2595, 2015.

[29] C. S. Park, V. R. Shrestha, S. S. Lee, E. S. Kim, and D. Y. Choi, "Omnidirectional color filters capitalizing on a nano-resonator of Ag-TiO_2-Ag integrated with a phase compensating dielectric overlay," *Sci. Rep.*, vol. 5, p. 8467, Feb. 2015.

[30] G. Kajtár, M. Kafesaki, E. N. Economou, and C. M. Soukoulis, "Theoretical model of homogeneous metal–insulator–metal perfect multi-band absorbers for the visible spectrum," *J. Phys. D, Appl. Phys.*, vol. 49, no. 5, p. 055,104, 2016.

[31] F. Ding, L. Mo, J. Zhu, and S. He, "Lithography-free, broadband, omnidirectional, and polarization-insensitive thin optical absorber," *Appl. Phys. Lett.*, vol. 106, p. 061,108, Feb. 2015.

[32] Y. K. Zhong et al., "Omnidirectional, polarization-independent, ultra-broadband metamaterial perfect absorber using field-penetration and reflected-wave-cancellation," *Opt. Exp.*, vol. 24, no. 10, p. A832, 2016.

[33] Y. K. Zhong et al., "Fully planarized perfect metamaterial absorbers with no photonic nanostructures," *IEEE Photon. J.*, vol. 8, no. 1, p. 2,200,109, 2016.

[34] S. M. Fu, Y. K. Zhong, M. H. Tu, B. R. Chen, and A. Lin, "A fully functionalized metamaterial perfect absorber with simple design and implementation," *Sci. Rep.*, vol. 6, p. 36,244, Oct. 2016.

[35] A. Ghobadi, S. A. Dereshgi, H. Hajian, B. Bozok, B. Butun, and E. Ozbay, "Ultra-broadband, wide angle absorber utilizing metal insulator multilayers stack with a multi- thickness metal surface texture," *Sci. Rep.*, vol. 7, p. 4755, July 2017.

[36] A. Ghobadi, H. Hajian, S. A. Dereshgi, B. Bozok, B. Butun, and E. Ozbay, "Disordered nanohole patterns in metal-insulator multilayer for ultra-broadband light absorption: Atomic layer deposition for lithography free highly repeatable large scale multilayer growth," *Sci. Rep.*, vol. 7, p. 15,079, Nov. 2017.

[37] S. Abedini Dereshgi, A. Ghobadi, H. Hajian, B. Butun, and E. Ozbay, "Ultra-broadband, lithography-free, and large-scale compatible perfect absorbers: The optimum choice of metal layers in metal-insulator multilayer stacks," *Sci. Rep.*, vol. 7, no. 1, Nov. 2017. doi: 0.1038/s41598-017-13837-8.

[38] K.-T. Lee, S. Seo, J. Y. Lee, and L. J. Guo, "Strong resonance effect in a lossy medium-based optical cavity for angle robust spectrum filters," *Adv. Mater.*, vol. 26, no. 36, pp. 6324–6328, 2014.

[39] J. H. Han, D.-Y. Kim, D. Kim, and K. C. Choi, "Highly conductive and flexible color filter electrode using multilayer film structure," *Sci. Rep.*, vol. 6, p. 29,341, July 2016.

[40] K. T. Lee, S. Seo, J. Yong Lee, and L. Jay Guo, "Ultrathin metal-semiconductor-metal resonator for angle invariant visible band transmission filters," *Appl. Phys. Lett.*, vol. 104, no. 23, p. 231,112, 2014.

[41] C. Yang et al., "Compact multilayer film structure for angle insensitive color filtering," *Sci. Rep.*, vol. 5, p. 9285, Mar. 2015.

[42] K. T. Lee, S. Y. Han, and H. J. Park, "Omnidirectional flexible transmissive structural colors with high-color-purity and high-efficiency exploiting multicavity resonances," *Adv. Opt. Mater.*, vol. 5, no. 14, p. 1,700,284, 2017.

[43] Z. Li, S. Butun, and K. Aydin, "Lithography-free transmission filters at ultraviolet frequencies using ultra-thin aluminum films," *J. Opt.*, vol. 18, no. 6, p. 065,006, 2016.

[44] Y. Zhao et al., "Artificial structural color pixels: A review," *Materials (Basel)*, vol. 10, no. 8, p. 944, 2017.

[45] A. Ghobadi, H. Hajian, A. R. Rashed, B. Butun, and E. Ozbay, "Tuning the metal filling fraction in metal-insulator-metal ultra-broadband perfect absorbers to maximize the absorption bandwidth," *Photon. Res.*, vol. 6, no. 3, p. 168, 2018.

[46] A. Ghobadi, H. Hajian, M. Gokbayrak, B. Butun, and E. Ozbay, "Bismuth-based metamaterials: From narrowband reflective color filter to extremely broadband near perfect absorber," *Nanophotonics*, vol. 8, no. 5, pp. 823–832, 2019.

[47] M. A. Kats, R. Blanchard, P. Genevet, and F. Capasso, "Nanometre optical coatings based on strong interference effects in highly absorbing media," *Nat. Mater.*, vol. 12, no. 1, pp. 20–24, 2012.

[48] J. Park et al., "Omnidirectional near-unity absorption in an ultrathin planar semiconductor layer on a metal substrate," *ACS Photon.*, vol. 1, no. 9, pp. 812–821, 2014.

[49] F. F. Schlich and R. Spolenak, "Strong interference in ultrathin semiconducting layers on a wide variety of substrate materials," *Appl. Phys. Lett.*, vol. 103, no. 21, pp. 1–4, 2013, doi: 10.1063/1.4833537, [Online]. Available: https://aip.scitation.org/doi/10.1063/1.4833537

[50] S. S. Mirshafieyan, H. Guo, and J. Guo, "Zeroth order Fabry–Perot resonance enabled strong light absorption in ultrathin silicon films on different metals and its application for color filters," *IEEE Photon. J.*, vol. 8, no. 5, p. 6,804,912, 2016.

[51] D. Liu, H. Yu, Y. Duan, Q. Li, and Y. Xuan, "New insight into the angle insensitivity of ultrathin planar optical absorbers for broadband solar energy harvesting," *Sci. Rep.*, vol. 6, no. 32,515, pp. 1–8, 2016.

[52] H. Song et al., "Nanocavity enhancement for ultra-thin film optical absorber," *Adv. Mater.*, vol. 26, no. 17, pp. 2737–2743, 2014.

[53] D. Liu and L. Wang. Designing planar, ultrathin, broad-band and material-versatile solar absorbers via bound-electron and exciton absorption. 2017. [Online]. Available: https://arxiv.org/abs/1710.06550

[54] E. Palacios, S. Park, S. Butun, L. Lauhon, and K. Aydin, "Enhanced radiative emission from monolayer MoS_2 films using a single plasmonic dimer nanoantenna," *Appl. Phys. Lett.*, vol. 111, no. 3, p. 031,101, 2017.

[55] Z. Liu and K. Aydin, "Localized surface plasmons in nanostructured monolayer black phosphorus," *Nano Lett.*, vol. 16, no. 6, pp. 3457–3462, 2016.

[56] J. Zheng, R. A. Barton, and D. Englund, "Broadband coherent absorption in chirped-planar-dielectric cavities for 2D-material-based photovoltaics and photodetectors," *ACS Photon.*, vol. 1, no. 9, pp. 768–774, 2014.

[57] H. Lu, X. Gan, D. Mao, Y. Fan, D. Yang, and J. Zhao, "Nearly perfect absorption of light in monolayer molybdenum disulfide supported by multilayer structures," *Opt. Exp.*, vol. 25, no. 18, pp. 21,630–21,636, 2017.

[58] C. Zhu, J. Li, Y. Yang, J. Huang, Y. Lu, and X. Zhao, "SiO_2/bi-layer GZO/Ag structures for near-infrared broadband wide-angle," *J. Phys. D, Appl. Phys. Papers*, vol. 49, no. 42, p. 425,106, 2016.

[59] H. Zheng et al., "Optical properties of Al-doped ZnO films in the infrared region and their absorption applications," *Nanoscale Res. Lett.*, vol. 13, no. 149, pp. 1–7, 2018.

[60] X. Wang, X. Jiang, Q. You, J. Guo, X. Dai, and Y. Xiang, "Tunable and multichannel terahertz perfect absorber due to Tamm surface plasmons with graphene," *Photon. Res.*, vol. 5, no. 6, pp. 536–542, 2017.

[61] Y. Chang et al., "Realization of mid-infrared graphene hyperbolic metamaterials," *Nat. Commun.*, vol. 7, p. 10,568, Feb. 2016.

[62] K. Shi, F. Bao, and S. He, "Enhanced near-field thermal radiation based on multilayer graphene-hBN heterostructures," *ACS Photon.*, vol. 4, no. 4, pp. 971–978, 2017.

[63] H. Hajian, A. Ghobadi, S. A. Dereshgi, B. Butun, and E. Ozbay, "Hybrid plasmon-phonon polariton bands in graphene-hexagonal boron nitride metamaterials [Invited]," *J. Opt. Soc. Amer. B*, vol. 34, no. 7, pp. D29–D35, 2017.

[64] H. Hajian, A. Ghobadi, B. Butun, and E. Ozbay, "Nearly perfect resonant absorption and coherent thermal emission by hBN-based photonic crystals," *Opt. Exp.*, vol. 25, no. 25, pp. 31970–31987, 2017.

[65] V. Steenhoff, M. Theuring, M. Vehse, and K. Von Maydell, "Ultrathin resonant-cavity-enhanced solar cells with amorphous germanium absorbers," *Adv. Opt. Mater*, vol. 3, no. 2, pp. 182–186, 2015.

[66] Q. Liu, P. Romero-Gomez, P. Mantilla-Perez, S. Colodrero, J. Toudert, and J. Martorell, "A two-resonance tapping cavity for an optimal light trapping in thin-film solar cells," *Adv. Energy Mater.*, vol. 7, no. 18, pp. 1–8, 2017, doi: 10.1002/aenm.201700356, [Online]. Available: https://onlinelibrary.wiley.com/doi/abs/10.1002/aenm.201700356

[67] Z. Xia et al., "Single-crystalline germanium nanomembrane photodetectors on foreign nanocavities," *Sci. Adv.*, vol. 3, no. 7, pp. 1–8, 2017, doi: 10.1126/sciadv.1602783, [Online]. Available: https://advances.sciencemag.org/content/3/7/e1602783

[68] A. Ghobadi, H. I. Yavuz, T. G. Ulusoy, K. C. Icli, M. Ozenbas, and A. K. Okyay, "Enhanced performance of nanowire-based all-TiO2 solar cells using subnanometer-thick atomic layer deposited ZnO embedded layer," *Electrochim. Acta*, vol. 157, pp. 23–30, Mar. 2015.

[69] A. Ghobadi, T. G. Ulusoy, R. Garifullin, M. O. Guler, and A. K. Okyay, "A heterojunction design of single layer hole tunneling ZnO passivation wrapping around TiO_2 nanowires for superior photocatalytic performance," *Sci. Rep.*, vol. 6, p. 30,587, 2016.

[70] A. Ghobadi, T. G. U. Ghobadi, F. Karadas, and E. Ozbay, "Angstrom thick ZnO passivation layer to improve the photoelectrochemical water splitting performance of a TiO_2 nanowire photoanode: The role of deposition temperature," *Sci. Rep.*, vol. 8, no. 1, p. 16,322, 2018.

[71] S. Butun and K. Aydin, "Functional metal-insulator-metal top contacts for Si-based color photodetectors," *J. Appl. Phys.*, vol. 120, no. 22, pp. 1–5, 2016.

[72] Q. Li et al., "Transmission enhancement based on strong interference in metal-semiconductor layered film for energy harvesting," *Sci. Rep.*, vol. 6, p. 29,195, July 2016.

[73] S. Y. Myong, S. S. Kim, and K. S. Lim, "Improvement of pin-type amorphous silicon solar cell performance by employing double silicon-carbide

p-layer structure," *J. Appl. Phys.*, vol. 95, no. 3, pp. 1525–1530, 2004.

[74] K. T. Lee, J. Y. Lee, S. Seo, and L. J. Guo, "Colored ultrathin hybrid photovoltaics with high quantum efficiency," *Light Sci. Appl.*, vol. 3, pp. 1–7, Oct. 2014, doi: 10.1038/lsa.2014.96, [Online]. Available: https://www.nature.com/articles/lsa201496

[75] D. Liu, L. Wang, Q. Cui, and L. J. Guo, "Planar metasurfaces enable high-efficiency colored perovskite solar cells," *Adv. Sci.*, vol. 5, no. 10, pp. 1–9, 2018, doi: 10.1002/advs.201800836, [Online]. Available: https://onlinelibrary.wiley.com/doi/full/10.1002/advs.201800836

[76] M. B. Upama et al., "Low-temperature processed efficient and colourful semitransparent perovskite solar cells for building integration and tandem applications," *Org. Electron.*, vol. 65, pp. 401–411, Feb. 2019.

[77] F. Liang et al., "Promising ITO-free perovskite solar cells with WO_3-Ag-SnO_2 as transparent conductive oxide," *J. Mater. Chem. A*, vol. 6, no. 40, pp. 19,330–19,337, 2018.

[78] K. T. Lee, J. Y. Jang, N. Y. Ha, S. Lee, and H. J. Park, "High-performance colorful semitransparent perovskite solar cells with phase-compensated microcavities," *Nano Res.*, vol. 11, no. 5, pp. 2553–2561, 2018.

[79] K. T. Lee, J. Y. Jang, S. J. Park, S. A. Ok, and H. J. Park, "Incident-angle-controlled semitransparent colored perovskite solar cells with improved efficiency exploiting a multilayer dielectric mirror," *Nanoscale*, vol. 9, no. 37, pp. 13,983–13,989, 2017.

[80] T. G. Ulusoy Ghobadi, A. Ghobadi, T. Okyay, K. Topalli, and A. K. Okyay, "Controlling luminescent silicon nanoparticle emission produced by nanosecond pulsed laser ablation: Role of interface defect states and crystallinity phase," *RSC Adv.*, vol. 6, no. 113, pp. 112520–112526, 2016.

[81] A. Ghobadi, T. Gamze, U. Ghobadi, A. K. Okyay, and E. Ozbay, "Emerging photoluminescence from defective vanadium diselenide nanosheets," *Photon. Res.*, vol. 6, no. 4, pp. 244–253, 2018.

[82] H. R. Rasouli, A. Ghobadi, T. G. U. Ghobadi, H. Ates, K. Topalli, and A. K. Okyay, "Nanosecond pulsed laser ablated sub-10 nm silicon nanoparticles for improving photovoltaic conversion efficiency of commercial solar cells," *J. Opt.*, vol. 19, no. 10, p. 105,902, 2017.

[83] K. X. Wang, Z. Yu, V. Liu, M. L. Brongersma, T. F. Jaramillo, and S. Fan, "Nearly total solar absorption in ultrathin nanostructured iron oxide for efficient photoelectrochemical water splitting," *ACS Photon.*, vol. 1, no. 3, pp. 235–240, 2014.

[84] H. Dotan et al., "Resonant light trapping in ultrathin films for water splitting," *Nat. Mater.*, vol. 12, no. 2, pp. 158–164, 2013.

[85] X. Yang, R. Liu, C. Du, P. Dai, Z. Zheng, and D. Wang, "Improving hematite-based photoelectrochemical water splitting with ultrathin TiO_2 by atomic layer deposition," *ACS Appl. Mater. Interfaces*, vol. 6, no. 15, pp. 12,005–12,011, 2014.

[86] J. P. McClure, K. N. Grew, D. R. Baker, E. Gobrogge, N. Das, and D. Chu, "Harvesting resonantly-trapped light for small molecule oxidation reactions at the Au/α-Fe_2O_3 interface," *Nanoscale*, vol. 10, no. 16, pp. 7833–7850, 2018.

[87] Y. Piekner et al., "Implementing strong interference in ultrathin film top absorbers for tandem solar cells," *ACS Photonics*, vol, 5, no. 12, pp. 5068–5078, 2018.

[88] J. Zhao et al., "High-performance ultrathin $BiVO_4$ photoanode on textured polydimethylsiloxane substrates for solar water splitting," *ACS Energy Lett*, vol. 1, no. 1, pp. 68–75, 2016.

[89] A. Kay et al., "Film flip and transfer process to enhance light harvesting in ultrathin absorber films on specular back-reflectors," *Adv. Mater.*, vol. 30, no. 35, pp. 1–7, 2018, doi: 10.1002/adma.201802781, [Online]. Available: https://onlinelibrary.wiley.com/doi/abs/10.1002/adma.201802781

[90] Y. H. Lee, J. Kim, and J. Oh, "Wafer-scale ultrathin, single-crystal Si and GaAs photocathodes for photoelectrochemical hydrogen production," *ACS Appl. Mater. Interfaces*, vol. 10, no. 39, pp. 33,230–33,237, 2018.

[91] T. G. U. Ghobadi, A. Ghobadi, E. Ozbay, and F. Karadas, "Strategies for plasmonic hot-electron-driven photoelectrochemical water splitting," *ChemPhotoChem*, vol. 2, no. 3, pp. 161–182, 2018.

[92] X. Shi, K. Ueno, T. Oshikiri, Q. Sun, K. Sasaki, and H. Misawa, "Enhanced water splitting under modal strong coupling conditions," *Nat. Nanotechnol.*, vol. 13, pp. 953–958, July 2018.

[93] Y. Lu, W. Dong, Z. Chen, A. Pors, Z. Wang, and S. I. Bozhevolnyi, "Gap-plasmon based broadband absorbers for enhanced hot-electron and photocurrent generation," *Sci. Rep.*, vol. 6, no. 30650, pp. 1–9, July 2016.

[94] F. Tan, N. Wang, D. Y. Lei, W. Yu, and X. Zhang, "Plasmonic black absorbers for enhanced photocurrent of visible-light photocatalysis," *Adv. Opt. Mater.*, vol. 5, no. 2, pp. 1–7, 2017, doi: 10.1002/adom.201600399, [Online]. Available: https://onlinelibrary.wiley.com/doi/abs/10.1002/adom.201600399

[95] L. Zhu, K. Liu, T. Hu, W. Dong, Z. Chen, and Z. Wang, "UV-visible photocurrent enhancement using metal-semiconductor-metal with symmetric and asymmetric double Schottky barriers," *Nanoscale*, vol. 10, no. 26, pp. 12,848–12,854, 2018.

[96] Z. Li, S. Butun, and K. Aydin, "Large-area, lithography-free super absorbers and color filters at visible frequencies using ultrathin metallic films," *ACS Photon.*, vol. 2, no. 2, pp. 183–188, 2015.

[97] Z. Fang et al., "Novel nanostructured paper with ultrahigh transparency and ultrahigh haze for solar cells," *Nano Lett.*, vol. 14, no. 2, pp. 765–773, 2014.

[98] K. T. Lee, C. Ji, D. Banerjee, and L. J. Guo, "Angular- and polarization-independent structural colors based on 1D photonic crystals," *Laser Photon. Rev.*, vol. 9, no. 3, pp. 354–362, 2015.

[99] C. Ji, K. T. Lee, T. Xu, J. Zhou, H. J. Park, and L. J. Guo, "Engineering light at the nanoscale: Structural color filters and broadband perfect absorbers," *Adv. Opt. Mater.*, vol. 5, no. 20, pp. 1–22, 2017.

[100] V. R. Shrestha, S. S. Lee, E. S. Kim, and D. Y. Choi, "Non-iridescent transmissive structural color filter featuring highly efficient transmission and high excitation purity," *Sci. Rep.*, vol. 4, p. 4921, May 2014.

[101] D. Fleischman, L. A. Sweatlock, H. Murakami, and H. Atwater, "Hyper-selective plasmonic color filters," *Opt. Exp.*, vol. 25, no. 22, pp. 27,386–27,395, 2017.

[102] B. Zeng, Y. Gao, and F. J. Bartoli, "Ultrathin nanostructured metals for highly transmissive plasmonic subtractive color filters," *Sci. Rep.*, vol. 3, p. 2840, Oct. 2013.

[103] M. J. Uddin and R. Magnusson, "Efficient guided-mode-resonant tunable color filters," *IEEE Photon. Technol. Lett.*, vol. 24, no. 17, pp. 1552–1554, 2012.

[104] Q. Wang et al., "Colored image produced with guided-mode resonance filter array," *Opt. Lett.*, vol. 36, no. 23, pp. 4698–4700, 2011.

[105] C.-T. Wang, P.-C. Chang, J. J. Lin, M. C. Tai, Y.-J. Hung, and T.-H. Lin, "Full-color reflector using vertically stacked liquid crystal guided-mode resonators," *Appl. Opt.*, vol. 25, no. 2, pp. 1248–1252, 2017.

[106] I. Koirala, V. R. Shrestha, C. S. Park, S. S. Lee, and D. Y. Choi, "Polarization-controlled broad color palette based on an ultrathin one-dimensional resonant grating structure," *Sci. Rep.*, vol. 7, p. 40,073, Jan. 2017.

[107] Y. Gu, L. Zhang, J. K. W. Yang, S. P. Yeo, and C.-W. Qiu, "Color generation *via* subwavelength plasmonic nanostructures," *Nanoscale*, vol. 7, no. 15, pp. 6409–6419, 2015.

[108] Q. Xiang, Y. Chen, and Y. Wang, "Plasmonic reflection color filters with metallic random nanostructures," *Nanotechnol.*, vol. 28, no. 8, p. 085,203, 2017.

[109] S. U. Lee and B.-K. Ju, "Wide-gamut plasmonic color filters using a complementary design method," *Sci. Rep.*, vol. 7, p. 40,649, 2017.

[110] G. Si et al., "Reflective plasmonic color filters based on lithographically patterned silver nanorod arrays," *Nanoscale*, vol. 5, no. 14, pp. 6243–6248, 2013.

[111] J. Wang et al., "Ultra-thin plasmonic color filters incorporating free-standing resonant membrane waveguides with high transmission efficiency," *Appl. Phys. Lett.*, vol. 110, no. 3, p. 031,110, 2017.

[112] Y.-T. Yoon, H.-S. Lee, S.-S. Lee, S. H. Kim, J.-D. Park, and K.-D. Lee, "Color filter incorporating a subwavelength patterned grating in poly silicon," *Opt. Exp.*, vol. 16, no. 4, pp. 2374–2380, 2008.

[113] M. J. Uddin, T. Khaleque, and R. Magnusson, "Guided-mode resonant polarization-controlled tunable color filters," *Opt. Exp.*, vol. 22, no. 10, pp. 12,307–12,315, 2014.

[114] Z. Yang et al., "Reflective color filters and monolithic color printing based on asymmetric Fabry–Perot cavities using nickel as a broadband absorber," *Adv. Opt. Mater.*, vol. 4, no. 8, pp. 1196–1202, 2016.

[115] A. Ghobadi, H. Hajian, M. C. Soydan, B. Butun, and E. Ozbay, "Lithography-free planar bandpass reflective color filter using series connection of cavities," *Sci. Rep.*, vol. 9, pp. 1–11, Jan. 2019.

[116] K. V. Sreekanth et al., "Biosensing with the singular phase of an ultrathin metal-dielectric nanophotonic cavity," *Nat. Commun.*, vol. 9, no. 1, pp. 1–8, 2018. doi: 10.1038/s41467-018-02860-6.

[117] S. Ayas, G. Bakan, E. Ozgur, K. Celebi, G. Torunoglu, and A. Dana, "Colorimetric detection of ultrathin dielectrics on strong interference coatings," *Opt. Lett.*, vol. 43, no. 6, pp. 2–5, 2018.

[118] M. Serhatlioglu, S. Ayas, N. Biyikli, A. Dana, and M. E. Solmaz, "Perfectly absorbing ultra thin interference coatings for hydrogen sensing," *Opt. Lett.*, vol. 41, no. 8, pp. 1724, 2016.

[119] S. Shinohara, D. Tanaka, K. Okamoto, and K. Tamada, "Colorimetric plasmon sensors with multilayered metallic nanoparticle sheets," *Chem. Phys.*, vol. 17, no. 28, pp. 18,606–18,612, 2015.

[120] N. Nath and A. Chilkoti, "Label-free biosensing by surface plasmon resonance of nanoparticles on glass: Optimization of nanoparticle size," *Anal. Chem.*, vol. 76, no. 18, pp. 5370–5378, 2004.

[121] J. M. M. M. de Almeida, H. Vasconcelos, P. A. S. Jorge, and L. Coelho, "Plasmonic optical fiber sensor based on double step growth of gold nano-islands," *Sensors*, vol. 18, no. 4, pp. 1–13, 2018.

[122] J. Liu, T. Wang, and F. Nie, "Narrow band resonance in the UV light region of a plasmonic nanotextured surface used as a refractive index sensor," *RSC Adv.*, vol. 7, no. 57, pp. 35,957–35,961, 2017.

[123] M. Taguchi, T. Ogami, J. Ando, T. Fukuda, and A. Emoto, "Ag-coated submicron particles of polystyrene formed by dewetting process and their application in multi-functional biosensor-chips," *Colloids Surf. A Physicochem. Eng. Asp.*, vol. 558, pp. 171–178, Dec. 2018.

[124] A. H. Thilsted et al., "Lithography-free fabrication of silica nanocylinders with suspended gold nanorings for LSPR-based sensing," *Small*, vol. 12, no. 48, pp. 6745–6752, 2016.

[125] H. Song et al., "Ultrathin-film titania photocatalyst on nanocavity for CO_2 reduction with boosted catalytic efficiencies," *Global Challenges*, vol. 2, no. 11, 2018, doi: 10.1002/gch2.201800032, [Online]. Available: https://onlinelibrary.wiley.com/doi/full/10.1002/gch2.201800032

N